NIH Public Access
Author Manuscript

Synaptic Vesicle Dynamics in Mouse Rod Bipolar Cells

Qun-Fang Wan[1], **Alejandro Vila**[1], **Zhen-yu Zhou**[1,2], and **Ruth Heidelberger**[1,*]

[1]*Department of Neurobiology and Anatomy, University of Texas Medical School at Houston, Houston, TX, 77030*

Abstract

To better understand synaptic signaling at the mammalian rod bipolar cell terminal and pave the way for applying genetic approaches to the study of visual information processing in the mammalian retina, synaptic vesicle dynamics and intraterminal calcium were monitored in terminals of acutely isolated mouse rod bipolar cells and the number of ribbon-style active zones quantified. We identified a releasable pool, corresponding to a maximum of ≈ 35 vesicles/ribbon-style active zone. Following depletion, this pool was refilled with a time constant of ≈ 7 s. The presence of a smaller, rapidly-releasing pool and a small, fast component of refilling were also suggested. Following calcium channel closure, membrane surface area was restored to baseline with a time constant that ranged from 2 to 21 seconds, depending upon the magnitude of the preceding Ca^{2+} transient. In addition, a brief, calcium-dependent delay often preceded the start of onset of membrane recovery. Thus, several aspects of synaptic vesicle dynamics appear to be conserved between rod-dominant bipolar cells of fish and mammalian rod bipolar cells. A major difference is that the number of vesicles available for release is significantly smaller in the mouse rod bipolar cell, both as a function of the total number per neuron and on a per active zone basis.

Keywords

exocytosis; endocytosis; ribbon synapse; retina; vesicle

Introduction

Chemical synaptic transmission is a fundamental mechanism by which neurons of the central nervous system communicate. Bipolar cells are glutamatergic retinal neurons that respond to stimuli with graded changes in membrane potential. These neurons make ribbon-style synapses and play a pivotal role in the transfer of visual information across the vertebrate retina. For the rod-dominant (Mb1) bipolar cell of the goldfish retina, there is a wealth of information available about synaptic vesicle dynamics and neurotransmitter release (Heidelberger *et al*., 1994; von Gersdorff & Matthews, 1994a; Heidelberger, 2001; Zenisek *et al*., 2004; Heidelberger *et al*., 2005; Sterling & Matthews, 2005). By contrast, relatively little is know about synaptic vesicle dynamics at mammalian bipolar cells. Such information would be valuable not only for gaining a better understanding of retinal signal processing, but also for the development of the mouse rod bipolar cell as a model system for understanding synaptic mechanisms at ribbon-style synapses.

*Corresponding author: Ruth Heidelberger, Department of Neurobiology and Anatomy, MSB 7.046, University of Texas Medical School at Houston, 6431 Fannin Street, Houston, Texas 77025, Phone: 713-500-5624, Fax: 713-500-0621, Email: ruth.heidelberger@uth.tmc.edu.

[2]Current address: Department of Cell Biology & Anatomy, New York Medical College, Basic Sciences Building, Rm 216, Valhalla, NY 10595

The mammalian rod bipolar cell is part of a high-sensitivity neural circuit specialized for scotopic vision that is unique to mammals and experiences a different synaptic demand than the goldfish Mb1 bipolar cell. While the Mb1 bipolar cell receives inputs from both rods and cones and makes chemical synapses directly onto third-order neurons (Stell *et al*., 1977; Ishida *et al*., 1980; Joselevitch & Kamermans, 2007), the rod bipolar cell receives input from rods and indirectly provides an output signal to ganglion cells, by first making chemical synapses onto AII amacrine cells that are electrically-couple via gap junctions to each other and to cone bipolar cells, which then make chemical synapses onto ganglion cells (Bloomfield & Dacheux, 2001; Tsukamoto *et al*., 2001; Veruki & Hartveit, 2002). The light response of the Mb1 bipolar cell is characterized by a sustained depolarization at low stimulus intensities that develops an initial, transient component as stimulus intensity increases (Saito & Kujiraoka, 1982; Joselevitch & Kamermans, 2007). Under some conditions, the response may even become regenerative (Protti *et al*., 2000). In response to a sustained depolarization, there is an initial burst of release from the Mb1 bipolar cell that is followed by a prominent, longer-lived secondary component of release (Sakaba *et al*., 1997; von Gersdorff *et al*., 1998). Both sustained and transient components of light-evoked release are also observed in neurons postsynaptic to the mammalian rod bipolar cell (Nelson, 1982; Kolb & Nelson, 1983; Dacheux & Raviola, 1986; Bloomfield & Xin, 2000; Pang *et al*., 2004). However, in response to a sustained depolarizing voltage-step, the transient component of the postsynaptic current is quite pronounced, while the sustained component is of relatively low amplitude (Singer & Diamond, 2003; Veruki *et al*., 2003; Trexler *et al*., 2005). This pattern is observed even in the presence of blockers of inhibitory GABAergic input and when only sustained calcium currents are activated in the rod bipolar cell, leading to the suggestion that glutamate release from the mammalian rod bipolar cell is inherently transient (Bieda & Copenhagen, 2000; Singer & Diamond, 2003). For all of these reasons, it is not clear to what extent information about synaptic vesicle pools and refilling dynamics obtained in Mb1 bipolar cells of the goldfish apply to the mammalian rod bipolar cell.

In a previous report, we demonstrated that under carefully-controlled conditions it is feasible to track synaptic vesicle dynamics in the mouse rod bipolar cell using time-resolved capacitance measurements, and we identified a pool of releasable synaptic vesicles (Zhou *et al*., 2006). In the present study, we extended these results by suggesting the presence of a small, rapidly-releasing pool, presumably representing those vesicles nearest the calcium channels (Mennerick & Matthews, 1996; Neher, 1998), and by characterizing the depletion and refilling rates of the 30 fF releasable vesicle pool. In addition, we quantified the number of ribbon-style active zones to allow the estimation of the mean number of vesicles in the releasable pool at each ribbon-style active zone of the mouse rod bipolar cell. Our results demonstrate that although the releasable pool of the mammalian rod bipolar cell per active zone is significantly smaller than that of the Mb1 bipolar cell of the goldfish (von Gersdorff *et al*., 1996; Sterling & Matthews, 2005), potentially contributing to an earlier depletion in the face of a prolonged or strong stimulus, the depletion and the refilling rates of this pool are similar to those reported for other ribbon synapses, including the Mb1 bipolar cell (von Gersdorff & Matthews, 1994a; 1997; Moser & Beutner, 2000; Heidelberger *et al*., 2002a; Eisen *et al*., 2004; Thoreson *et al*., 2004; Rabl *et al*., 2005). In addition, although the time course of membrane recovery did not exhibit a fast component, the major component of membrane recovery had a comparable time course to that observed in the Mb1 bipolar cell (von Gersdorff & Matthews, 1997; Neves & Lagnado, 1999; Neves *et al*., 2001). Thus, despite their different connectivity, several aspects of synaptic vesicle dynamics are similar between the mouse rod bipolar cell and the rod-dominant bipolar cell of the fish. The extent to which the molecular mechanisms underlying these processes are conserved remains to be seen.

Methods

Cell isolation

Rod bipolar cells were isolated from 2-6 month old C57Bl6/J mice by mechanical trituration after enzymatic digestion, using methods similar to those previously described (Zhou *et al.*, 2006). All animal procedures conformed to NIH guidelines and were approved by the Animal Welfare Committee of the University of Texas Health Science Center at Houston. In brief, animals were euthanized and the retinas rapidly removed and placed in cold, oxygenated, low–calcium modified Hanks' solution (in mM): NaCl, 138; $CaCl_2$, 0.5; $MgCl_2$, 0.5; $MgSO_4$, 0.4; KCl, 5; KH_2PO_4, 0.44; Na_2HPO_4, 0.34; D-Glucose, 10; HEPES, 10; adjusted to PH 7.2, 310–315 mOsm. Then, each retina was cut into 6-8 small pieces and incubated for 20-25 min at room temperature in an enzymatic solution that consisted of the low-calcium Hanks' saline described above, supplemented with 2.7 mM L-cysteine (Sigma) and 30 U/ml papain (Fluka). After being rinsed in low-calcium Hanks' solution, pieces were stored in an oxygenated environment at 10°C for $\leq$ 8 hours prior to mechanical trituration with a fire-polished Pasteur pipette. The resulting cell suspension was plated onto clean glass cover slips. Rod bipolar cells were identified based on their characteristic morphology using previously described criteria (Zhou *et al.*, 2006).

Electrophysiological and intraterminal Ca^{2+} measurements

Whole-cell capacitance measurements were performed with a 5-6 MΩ pipette placed on the soma of an intact rod bipolar cell at 21-24°C (Zhou et al., 2006). Capacitance measurements were made with the use of an EPC-9 patch-clamp amplifier together with PULSE LOCK-IN software (Heka Electronics, Lambrecht, Germany). An 800-Hz, 30-mV peak-to-peak sinusoidal voltage stimulus was superimposed on a holding potential of -70 mV. Currents were filtered at 2.9 kHz. The resultant signal was processed using the Lindau-Neher technique to yield estimates of C_m, G_m, and G_s. For high-resolution measurements, one data point for C_m, G_m, and G_s was generated per sine wave cycle. For time-resolved measurements, the average values obtained from each 100 ms sweep were recorded. For both types of measurements, capacitance changes were not measured during the depolarization. The intracellular solution typically contained (mM): 125 Cs-gluconate, 10 TEA-Cl, 3 $MgCl_2$, 2 Na_2ATP, 0.5 GTP, 0.1 EGTA, 0.2 bis-fura-2, 35 HEPES, pH = 7.2, 310 - 315 mOsm. In some experiments, where indicated, the EGTA concentration in the internal solution was 0.5 mM. Bis-fura-2 was chosen over fura-2 as the indicator dye because of its higher fluorescent yield and K_d of $\approx$ 500 nM under physiological conditions (Naraghi *et al.*, 1998). The external recording solution contained (mM): 127 NaCl, 5 CsCl, 20 TEA-Cl, 1 $MgCl_2$, 2 $CaCl_2$, 10 glucose, and 10 HEPES, pH = 7.4, 315 - 320 mOsm.

For measurement of intraterminal Ca^{2+}, alternating excitation at 340 nm and 385 nm was provided by a computer-controlled monochrometer-based system (ASI/T.I.L.L. Photonics) (Messler *et al.*, 1996). The resulting fluorescence signal was captured by a photomultiplier (R928; Hamamatsu Phototonics, Hamamatsu City, Japan). An adjustable aperture was used to position the collection field for emitted fluorescence selectively over the terminal cluster (Zhou *et al.*, 2006). Intraterminal Ca^{2+} was determined from the ratio (R) of the fluorescence signals excited at the two wavelengths, following the equation $[Ca^{2+}]_i = K_{eff} * (R-R_{min})/(R_{max}-R)$, where K_{eff}, R_{min}, and R_{max} are constants obtained from an in vivo calibration as previously described (Heidelberger & Matthews, 1992). In brief, three solutions with a Ca^{2+} concentrational of nominal zero (10 mM EGTA with no added Ca^{2+}), 300 nM (3.3 mM EGTA with 6.6 mM CaEGTA), and 10 mM (10 mM $CaCl_2$ with no added buffer) were dialyzed against the cytosol in the whole-cell patch clamp recording. Three to five recordings were made for each calibration solution.

Cells in which the terminals escaped voltage control, as judged from the Ca^{2+} records, were excluded from analysis. Also excluded from analysis were cells with leak currents larger than 30 pA or access resistances > 35ΩM (Zhou *et al*., 2006). The average leak current was 20.6 ± 1.1 pA and the average value of the access resistance, R_s, was 30 ± 0.6 MΩ and (n=157). All data was imported to IGOR Pro (WaveMetrics) for further analysis.

Immunocytochemistry and confocal microscopy

Following euthanasia, the eyes were enucleated, and the anterior chamber and lens were removed. The eyecups were immersion-fixed in 4% (w/v) paraformaldehyde (PFA) in 0.1 M phosphate buffer (PB), pH 7.4, for 15-30 min, cryoprotected in graded/30% sucrose, embedded in OCT embedding medium, fast frozen, and then sectioned vertically at 12-14 μm on a cryostat onto gelatin-coated slides and stored at -20°C until use. In some cases, the whole retina was also isolated and stored in PB at 4°C until antibody staining. For single bipolar cells, fixation was begun after letting cells settle for 15–30 min onto glass coverslips coated with 0.1 mg/ml poly-D-lysine and attach for 10-15 min at 6-8°C. After rinsing with PB, cells were stored in PB at 4°C until antibody staining.

Immunostaining was performed using the indirect fluorescence method. Briefly, retinal sections and dissociated cells were incubated with primary antibodies diluted in 3% NGS, 1% BSA, 0.5% Triton X-100, 0.05% NaN3, 0.1M PB, overnight at 4°C. Whole mount preparations were incubated in primary antibody for 7 days at 4°C. Primary antibodies used were ① rabbit polyclonal antibody anti-protein kinase C (Calbiochem, San Diego, CA) at dilution 1:1000, as a marker of rod bipolar cells (Wang *et al*., 2003) and ② ribbon-specific mouse monoclonal antibody anti- CtBP2/ribeye, dilution 1:200 (BD Transduction Laboratories, San Jose, CA, 612044). For fluorescence labeling, cells were incubated with a mixture of Alexa-tagged anti-mouse (488 nM) and anti-rabbit (568 nM) IgG secondary antibodies (Molecular Probes, Eugene, OR, USA) at 1:1000 dilutions for 1hr at room temperature in a light-protected environment. Cells were rinsed, mounted on a slide with anti-fade mounting medium (Molecular Probes).

Immunolabeled specimens were scanned with a 0.2 μm step size on a Zeiss Laser Scanning Microscope 510 Meta (Carl Zeiss, Inc., Thornwood, NY, USA) with a Zeiss 40× 1.3 NA Plan-NEOFLUAR oil objective. Confocal images were analyzed using the Zeiss LSM 510 proprietary software. Intensity levels and brightness/contrast were adjusted in Adobe Photoshop CS v.8.0 (Adobe Systems, San Jose, CA). The number of active zones was quantified in projected confocal stack (0.2 μm step size) obtained from each mouse bipolar cell double-labeled with antibodies against PKC and CtBP2/ribeye. Only CtBP2 fluorescent signals present within PKC-α- positive terminals were counted.

Data Analysis

Data analysis was performed using IGOR Pro software (Wavemetrics), and results were presented as mean ± SEM, where n indicates the number of experiments. The increase in membrane capacitance, ΔC_m, evoked by depolarization was calculated as $\Delta C_m = C_{m (response)}-C_{m (rest)}$. $C_{m(rest)}$ was defined as the average C_m value during the 30 ms before the depolarization step, obtained from the high-resolution record, or 5 s before the depolarization step, obtained from the time-resolved record; both gave equivalent measures of $C_{m(rest)}$. $C_{m (response)}$ was calculated following a 25 ms interval that was not evaluated due to potential complications associated with gating currents and/or the decay of depolarization-evoked conductance changes (Horrigan & Bookman, 1994; Gillis, 1995). The increase in the spatially-averaged intraterminal calcium, ΔCa, was typically measured as $\Delta Ca = Ca_{(peak)}-Ca_{(rest)}$, where $Ca_{(peak)}$ was the first calcium measurement immediately after the depolarization, and $Ca_{(rest)}$ was the average Ca^{2+} value measured over the 5 s before the voltage

step. For paired-pulse experiments in which the interpulse interval was ≤ 2.02 s, $Ca_{(peak)}$ measurements and $Ca_{(rest)}$ for the second depolarization were taken from the high-resolution data. To measure the delay in the onset of membrane recovery, for each record, the magnitude of the capacitance response after channel closure and prior to the onset of endocytosis was determined. Then, the falling phase of the capacitance response was fit with a single exponential function. The delay in the onset of membrane recovery was defined as the interval between the cessation of the depolarization and the time at which the exponential fit achieved the magnitude of the capacitance response. A simple regression analysis was performed using SAS 9.1 software (Cary, N.C.).

Results

A rod bipolar cell contains ≈ 34 ribbon-style active zones

To be able to correlate the number of anatomical ribbon-style active zones with the magnitude of the releasable pool, we analyzed the number of ribbon-style active zones of the mouse rod bipolar cell using an immunocytochemical approach in combination with confocal microscopy. Synaptic ribbons were identified by immunostaining for CtBP2/ribeye, a structural element of the synaptic ribbon(Schmitz *et al*., 2000; tom Dieck *et al*., 2005), shown in green in Figures 1A, 1D, and 1G. Rod bipolar cells were identified by red labeling with an antibody directed against protein kinase C alpha (PKC-α) (Wang *et al*., 2003) in Figures 1B, 1E, and 1H. The merged images from PKC-α and CtBP2/ribeye double-labeled cells (Figures 1C, 1F, and 1I) reveal that CtBP2 immunofluorescence (green) is prominent in the synaptic terminals of rod bipolar cells and in the inner plexiform layer of the retina (IPL), as expected. The number of active zones was quantified from a projected confocal stack of CtBP2 fluorescent puncta within PKC-α-positive terminals. The mean number of ribbon-style active zones per terminal cluster was 34 ± 4 (n=10). This value falls within the range of ribbon-style active zones suggested for rod bipolar cells of several mammalian species (Tsukamoto *et al*., 2001; Singer *et al*., 2004; Sterling & Matthews, 2005; LoGiudice *et al*., 2008)

Depletion of the releasable pool

Previously, we have verified the use of capacitance measurements for the study of exocytosis in dissociated mouse rod bipolar cells and used this approach to identify a pool of releasable synaptic vesicles (Zhou *et al*., 2006). Here, we extend these results be studying both the depletion and refilling rate of this pool of vesicles. A typical example of a high resolution capacitance record from dissociated mouse rod bipolar cell is shown in Figure 2A. A 1 s depolarization from -70 to 0 mV was given (first vertical dashed line). Following the cessation of the pulse, there is a ≈ 38 fF increase in membrane capacitance (C_m). There were no correlated changes in the conductance records (G_m and G_s), indicating that the change in capacitance was real. Figure 2B shows the low time resolution capacitance and calcium records for the same neuron. The average free Ca^{2+} concentration of a bipolar terminal held at -70 mV was 49.4 ± 3.0 nM (n = 157).

The first step towards quantifying the kinetics of depletion and refilling of the releasable pool of this neuron was to compare the magnitude of the depolarization-evoked capacitance change as a function of pulse duration (100 - 5000 ms) for a fixed-amplitude depolarization (-70 to 0 mV). Figure 2C demonstrates that the amplitude of C_m increases with pulse duration until a pulse duration of ≈ 1 s, where it reaches a plateau value of 29 ± 2 fF (n=43), indicative of the releasable pool of vesicles (Zhou *et al*., 2006). To calculate the rate of depletion, the data were fit with a single exponential function, yielding a time constant of ≈ 417 ms (Figure 2C, dotted line). The y-intercept of this fit was not zero, but rather 3.8 fF, suggesting that in addition to the releasable pool, the mouse rod bipolar cell might also possess a small, rapidly-releasing pool (e.g. Mennerick & Matthews, 1996).

An important caveat with the above definition of the releasable pool is that it assumes that the amount of calcium entry is linearly related to pulse duration. Therefore, we additionally analyzed the increase in C_m as a function of the depolarization-evoked increase in intraterminal Ca^{2+} ($\Delta[Ca^{2+}]_i$) (Figure 2C). $\Delta[Ca^{2+}]_i$, measured selectively from the terminal cluster (Zhou *et al*., 2006) was used rather than the integral of I_{Ca}^{2+} because under physiological conditions, the maximum amplitude of I_{Ca}^{2+} is quite small and thus, difficult to accurately measure (De la Villa *et al*., 1998). As can be seen in Figure 2D, despite the larger increase in $\Delta[Ca^{2+}]_i$ evoked by 5 s pulse relative to the 1 s pulse, the increase in membrane capacitance was similar. Thus, the plateau in ΔC_m was not caused by a plateau in the depolarization-evoked Ca^{2+} signal, indicating that the measured depletion rate most likely represents the depletion rate of the releasable pool of vesicles (see also Zhou *et al*., 2006). Interestingly, the average Ca^{2+} responses to the 1 s and 2 s depolarizations were similar in amplitude, highlighting the importance of measuring either Ca^{2+} entry or Ca^{2+} elevation when estimating pool sizes. Whether this similarity reflects the contributions of Ca^{2+}-dependent Ca^{2+} channel inactivation (von Gersdorff and Matthews 1996), a transient Ca^{2+} channel (e.g. Pan et al., 2001), and/or Ca^{2+}-handling mechanisms that may be overcome with longer depolarizations is not yet known. Never-the-less, the data demonstrate that a 1 s depolarization (70 to 0 mV) is sufficient to deplete the entire releasable pool without appreciably tapping vesicle recruitment.

Time course of recovery from paired-pulse depression

Following exocytosis, vesicles in the releasable pool must be replaced in order to allow subsequent responses to appropriate stimuli. To measure the time course of pool refilling, two successive 1 s pulses from -70 to 0 mV with a variable interpulse interval were given. The first 1 s depolarization emptied the entire releasable pool, and the second depolarizing stimulus evaluated the extent of pool refilling. In Figure 3A, the second depolarizing stimulus followed the first by 5.2 s, and the amplitude of the second C_m jump was only 21% of the first. When the interpulse interval was increased to 12.1 s, the amplitude of the second C_m jump recovered to 72% of the first (Figure 3B). In both cases, the corresponding intraterminal Ca^{2+} increase elicited by the two successive pulses were similar, excluding changes in Ca^{2+} entry as a mechanism underlying the observed depression of the secretory response. Figures 3C & D show the second C_m jump or the second rise in intraterminal Ca^{2+} as a percent of the first from a total of 60 such experiments. The time course of C_m recovery was described by a single exponential function with a time constant of ≈ 6.8 s (Figure 3D). The non-zero intercept of this fit suggests that there may also be a small, fast component of refilling. The time course of simultaneous measurement of intraterminal calcium Ca^{2+} recovery did not correlate with the time course of C_m recovery. Thus, the time course of C_m recovery most likely reflects the refilling time course of the releasable pool, rather than depression and recovery of Ca^{2+} signaling.

Recovery of C_m is retarded by large Ca^{2+} transients

To maintain cell surface area and normal synaptic transmission, membrane added via neurotransmitter exocytosis must be retrieved. In the dissociated mouse rod bipolar cell, membrane recovery typically followed exocytosis elicited by a 500 ms depolarization (Figures 4A & B). The time constant of membrane recovery, $\tau_{recovery}$, estimated from a single exponential fit to the recovery phase of membrane capacitance (Figures 4A & B; solid curve), ranged from 2 s to 21 s (mean = 5.92 ± 0.92 s, n=27).

In Figure 4A, a relatively small stimulus-evoked increase in intraterminal Ca^{2+} (304 nM) was associated with the rapid recovery of membrane capacitance ($\tau_{recovery} = 3.7$ s), whereas, membrane recovery was significantly slower ($\tau_{recovery} = 14.6$ s) when the Ca^{2+} transient reached 980 nM (Figure 4B). In goldfish Mb1 bipolar cells, the rate of membrane retrieval is sensitive to changes in the spatially-averaged, intraterminal Ca^{2+} (von Gersdorff & Matthews,

1994b; Neves & Lagnado, 1999; Heidelberger, 2001). To ascertain whether membrane recovery of the mouse rod bipolar cell might also be affected by intraterminal Ca^{2+}, for 27 neurons, the time constant of membrane recovery following a 500 ms depolarization was plotted as a function of the magnitude of the corresponding depolarization-evoked Ca^{2+} transient (Figure 4C). The relationship, described by a line with slope of ≈ 0.01 (p <0.001) and a correlation of determination, r^2, of ≈ 0.71, supports the observation that with an increase in the amplitude of the Ca^{2+} transient, the time course of membrane recovery is prolonged.

It appeared that the delay in the onset of membrane recovery might be longer following a larger Ca^{2+} transient (Figures 4A and B). To see whether this observation generally held true, the onset delay for each cell was plotted as a function of the magnitude of the preceding Ca^{2+} transient. Delays were calculated as described in Methods and depicted in Figure 4B (inset). As shown in Figure 4D, there was a minor correlation between the amplitude of the Ca^{2+} signal and the delay in the onset of membrane recovery (slope ≈ 0.002, p = 0.0003; $r^2 = 0.41$).

Discussion

The active zones of a bipolar cell are marked by the presence of the synaptic ribbon. One of the proposed roles for the synaptic ribbon is to hold a cohort of release-ready synaptic vesicles near the sites of vesicle fusion (Witkovsky & Dowling, 1969; Heidelberger, 1998; Zenisek *et al*., 2000; von Gersdorff, 2001; Sterling & Matthews, 2005). These vesicles have typically been divided into two distinct pools based upon their fusion kinetics and proximity to calcium channels (Mennerick & Matthews, 1996; von Gersdorff & Matthews, 1997; Gomis *et al*., 1999; Richards *et al*., 2003; Heidelberger *et al*., 2005; Wadel *et al*., 2007). The rapidly-releasing pool is thought to present those vesicles on the bottom-most row(s) of vesicles tethered to the ribbons and be in physical contact with the plasma membrane. These vesicles are often referred to as being "docked." By contrast, the releasable pool may represent the totality of ribbon-tethered vesicles and includes vesicles located at a variety of distances from the plasma membrane and presynaptic calcium channels. Thus, the average vesicle in the releasable pool would be expected to be released upon calcium channel activation with fusion kinetics that are slower, on average, than the average vesicle in the rapid pool.

In this study, we characterized the synaptic vesicle dynamics of the releasable vesicle pool in the mouse rod bipolar cell, extending a previous study demonstrating proof-of-principle for using capacitance measurements to monitor exocytosis in these neurons (Zhou *et al*., 2006). In the present study, we demonstrate that fusion of the entire releasable pool of vesicles is triggered by 1 s depolarization (-70 - 0 mV). Like the releasable pools at other ribbon synapses (Mennerick & Matthews, 1996; Neves & Lagnado, 1999; Eisen *et al*., 2004; Thoreson *et al*., 2004) and at peptidergic nerve terminals (Hsu & Jackson, 1996), the depletion rate was on the order of a few hundred milliseconds (Figure 2). This stands in contrast to the rapidly-releasing pool, which exhibits depletion with a time constant of a few milliseconds in rod-driven bipolar cells (Mennerick & Matthews, 1996; Singer & Diamond, 2006).

Although we could not directly measure a small, rapidly-releasing pool, the non-zero y-intercept of the fit to the data in Figure 2 imply the existence of such a small, fast pool. In addition, the y-intercept sets the lower estimate of the magnitude of this presumptive pool at ≈ 4 fF, while the magnitude of the capacitance increase at the shortest pulse duration, ≈ 10 fF, provides an upper limit. This range of magnitude for the presumptive rapidly-releasing pool is in agreement with the amplitude predicted for this pool of 6 fF, based upon a 5:1 ratio of the releasable to rapid pool (Sterling & Matthews, 2005;Zhou *et al*., 2006).

The average size of the releasable pool was ≈ 30 fF, consistent with previous results (Zhou *et al*., 2006). If this pool were evenly distributed across the 34 ribbon-style active zones (Figure

1), each active zone would possess ≈ 0.88 fF worth of releasable vesicles. Assuming a conversion factor of 25 aF/vesicle, obtained from the specific membrane capacitance of 9 fFμm^{-2} (Gentet *et al*., 2000) and a vesicle diameter of ≈ 30 nm (von Gersdorff *et al*., 1996; Spiwoks-Becker *et al*., 2001; Tsukamoto *et al*., 2001), the releasable pool of the mouse rod bipolar cell would correspond to nearly 1,200 vesicles or ≈ 35 vesicles per ribbon-style active zone. This is consistent with the predicted size of the releasable pool per ribbon synapse in the rat rod bipolar cell based upon data obtained from paired recordings (Singer & Diamond, 2006). In addition, the putative docked or rapidly-releasing pool would correspond to ≈ 8 vesicles per synaptic ribbon (assuming an average pool size of 7 fF), in agreement with the number of vesicles expected to give rise to the transient component of the rat AII light response (Singer & Diamond, 2006). However, there are some indications that the vesicle diameter in the mouse rod bipolar cell may be somewhat larger than the assumed 30 nm and perhaps as large as 35 - 50 nm, when the underestimation of object size in thin sections is addressed (D. Sherry, unpublished observations; estimation adjusted according to Abercrombie, 1946). In this case, the releasable pool would be predicted to be on the order of 425-900 vesicles per terminal and 12-25 vesicles per ribbon-style active zone. If the latter is correct, one prediction is that synaptic ribbons of the mouse rod bipolar cell should be smaller and tether fewer vesicles than in the rat. A detailed ultrastructural analysis of ribbon-style active zones in rod bipolar cells, which has not yet been performed in any mammalian species, would help distinguish between this and other possibilities.

The ability of a presynaptic terminal to maintain the supply of releasable vesicles is determined by the balance between the rate of pool depletion and the rate of pool refilling. In the present study, the releasable pool of vesicles in the mouse rod bipolar cell was depleted by a 1 s depolarization (-70 to 0 mV) and recovered with a time course described by a single exponential function with a time constant of ≈ 7 s (Figure 3). This is comparable to the major time course of pool refilling of the releasable pool in the rod-dominant bipolar cells of the goldfish measured under similar experimental conditions (von Gersdorff & Matthews, 1997;Heidelberger *et al*., 2002a;Hull *et al*., 2006). In addition, although we were unable to resolve the fast component of release, the presence of such a component was suggested by the non-zero intercept of the single exponential fit (Figure 3D). Thus, it may be that as at other ribbon-style synapses, the mouse rod bipolar cell releasable pool exhibits more than one kinetic component of pool refilling (Moser & Beutner, 2000;Edmonds *et al*., 2004;Hull *et al*., 2006).

Membrane added to the plasma membrane during exocytosis of neurotransmitter is retrieved through endocytosis. Membrane retrieval is crucial for vesicle recycling and for sustaining neurotransmitter release in synaptic terminals. Following exocytosis evoked by a 500 ms depolarization, membrane capacitance typically decayed back to the pre-stimulus baseline (Figures 2, 3, and 4), consistent with a tight regulation of membrane surface area in nerve terminals (von Gersdorff & Matthews, 1994a). The time constant of the recovery phase in the present study ranged from 2 to 21 s (Figure 4). This is comparable to the range of time constants reported for endocytosis in the goldfish Mb1 bipolar cell, which can exhibit a fast component (time constant 1~2 s) and/or a slower process (time constant 5~30 s), depending upon experimental conditions (von Gersdorff & Matthews, 1994a, 1997; Neves & Lagnado, 1999; Heidelberger, 2001; Neves *et al*., 2001; Heidelberger *et al*., 2002a). In the Mb1 bipolar cell, the two components of endocytosis represent distinct mechanisms of retrieval (Heidelberger *et al*., 2002a; Paillart *et al*., 2003; Jockusch *et al*., 2005). A fast component of membrane recovery was not resolvable in the present study, possibly because or signal-to-noise issues or continued neurotransmitter release following calcium channel closure (Pan *et al*., 2001; Singer & Diamond, 2003). Alternatively, it may be that under the conditions of the present study, retrieval occurs preferentially via a single pathway. If the fastest time course of is endocytosis is on the order of seconds, then the putative fast component of pool refilling may draw from a source of vesicles other than those that are newly retrieved. The ability to refill the releasable

pool directly from preformed vesicles has been suggested at other ribbon-style synapses (von Gersdorff & Matthews, 1997; Heidelberger *et al*., 2002b; Kreft *et al*., 2003; Eisen *et al*., 2004; Thoreson *et al*., 2004).

The regulation of endocytosis by calcium is complex. In some nerve terminals, the time course of endocytosis may be prolonged or even inhibited by elevated cytosolic calcium and/or activity (von Gersdorff & Matthews, 1994b; Hsu & Jackson, 1996; Wu & Betz, 1996; Rouze & Schwartz, 1998; Neves & Lagnado, 1999; Sun & Wu, 2001; Artalejo *et al*., 2002; Wu, 2004), despite the fact that Ca^{2+} may be important for initiating fast endocytosis (Neves et al., 2001). In the mouse rod bipolar cell, both the time constant of membrane recovery and the delay in the onset of recovery increased were correlated with the magnitude of the increase in intraterminal Ca^{2+} (Figure 4). These results are not readily explained by saturation of the endocytic machinery because there was no obvious relationship between the time constant of recovery and the magnitude of the capacitance jump (data not shown). Rather, the results are reminiscent of the effect of elevated bulk cytosolic calcium on membrane retrieval in goldfish Mb1 bipolar cells, in which a delay in onset and a prolongation of the retrieval time course, as measured by monitoring changes in membrane capacitance, were reported (von Gersdorff & Matthews, 1994b; Heidelberger 2001). That these effects were not caused by concurrent asynchronous release was demonstrated by Rouze and Schwartz (Rouze & Schwartz, 1998), who used an optical approach to track vesicle cycling and found the activation of calcium entry through voltage-gated calcium inhibited endocytosis in goldfish bipolar cells. Future studies, wherein exocytosis and endocytosis can be independently monitored, will be required to determine whether the calcium-dependent inhibition of recovery of membrane surface area in the mouse rod bipolar cell is caused by a similar calcium dependent inhibition of endocytosis or by a calcium-dependent increase in asynchronous release.

In summary, the combination of membrane capacitance measurements and measurements of intraterminal calcium has allowed us to perform a detailed characterization of synaptic vesicle dynamics in the mouse rod bipolar cell terminal. The kinetics of depletion and refilling of the releasable pool are comparable to that observed at other ribbon-style synapses measured under similar experimental conditions, including the goldfish Mb1 bipolar neuron. In addition, although the estimated number of releasable vesicles per active zone is ≈ 50 -70 % smaller in the mouse rod bipolar cell than that of the well-studied goldfish Mb1 bipolar cell (Sterling & Matthews 2005; von Gersdorff *et al*., 1996), the predicted ratios between the amplitudes of the rapidly-releasing pool and releasable pool are similar for the two neurons. Thus, several important aspects of synaptic vesicle dynamics are quantitatively conserved from fish to mammals. In both species, vesicles in the releasable pool are likely to contribute to a slower, more sustained component of neurotransmitter release, while the subset of docked vesicles is likely to contributed to a limited burst of release at light onset.

Finally, it is also important to note that the experiments reported here were performed at room temperature, facilitating comparisons with previous studies of synaptic vesicle dynamics performed in mammalian and non-mammalian bipolar cells. However, both membrane retrieval and pool refilling rates have been reported to be temperature-sensitive (Pyott & Rosenmund 2002; Kushmerick *et al*., 2006; Rendon & von Gersdorff 2007). Thus, it is conceivable that at physiological temperature, both membrane recovery and pool refilling in the mouse rod bipolar cell may be even faster than reported here. While these data on synaptic vesicle dynamics do not *a priori* suggest an inherently more transient pattern of neurotransmitter release from the mammalian rod bipolar cell relative to the goldfish Mb1 bipolar cell, resolution of the putative fast components of release and refilling is needed. Additional presynaptic mechanisms, including the calcium- and activity-dependent modulation of release, refilling and vesicle recycling, and the number and availability of reserve vesicles, will further sculpt synaptic output and the transmission of visual information.

Acknowledgements

References

Abercrombie M. Estimation of nuclear population from microtome sections. Anat Rec 1946;94:239–247.

Artalejo CR, Elhamdani A, Palfrey HC. Sustained stimulation shifts the mechanism of endocytosis from dynamin-1-dependent rapid endocytosis to clathrin- and dynamin-2-mediated slow endocytosis in chromaffin cells. Proc Natl Acad Sci USA 2002;99:6358–6363. [PubMed: 11959911]

Bieda MC, Copenhagen DR. Inhibition is not required for the production of transient spiking responses from retinal ganglion cells. Visual Neurosci 2000;17:243–254.

Bloomfield SA, Dacheux RF. Rod Vision: Pathways and Processing in the Mammalian Retina. Prog Retin Eye Res 2001;20:351–384. [PubMed: 11286897]

Bloomfield SA, Xin D. Surround inhibition of mammalian AII amacrine cells is generated in the proximal retina. J Physiol 2000;523(Pt 3):771–783. [PubMed: 10718754]

Dacheux RF, Raviola E. The rod pathway in the rabbit retina: a depolarizing bipolar and amacrine cell. J Neurosci 1986;6:331–345. [PubMed: 3950701]

De la Villa P, Vaquero CF, Kaneko A. Two types of calcium currents of the mouse bipolar cells recorded in the retinal slice preparation. Eur J Neurosci 1998;10:317–323. [PubMed: 9753140]

Edmonds BW, Gregory FD, Schweizer FE. Evidence that fast exocytosis can be predominantly mediated by vesicles not docked at active zones in frog saccular hair cells. J Physiol 2004;560:439–450. [PubMed: 15308677]

Eisen MD, Spassova M, Parsons TD. Large releasable pool of synaptic vesicles in chick cochlear hair cells. J Neurophysiol 2004;91:2422–2428. [PubMed: 14749306]

Gentet LJ, Stuart GJ, Clements JD. Direct Measurement of Specific Membrane Capacitance in Neurons. Biophys J 2000;79:314–320. [PubMed: 10866957]

Gillis, KD. Techniques for membrane capacitance measurements. In: Sakmann, B.; Neher, E., editors. single-channel recording. Plenum Press; New York and London: 1995. p. 155-198.

Gomis A, Burrone J, Lagnado L. Two actions of calcium regulate the supply of releasable vesicles at the ribbon synapse of retinal bipolar cells. J Neurosci 1999;19:6309–6317. [PubMed: 10414960]

Heidelberger R. Adenosine triphosphate and the late steps in calcium-dependent exocytosis at a ribbon synapse. J Gen Physiol 1998;111:225–241. [PubMed: 9450941]

Heidelberger R. ATP is required at an early step in compensatory endocytosis in synaptic terminals. J Neurosci 2001;21:6467–6474. [PubMed: 11517235]

Heidelberger R, Heinemann C, Neher E, Matthews G. Calcium dependence of the rate of exocytosis in a synaptic terminal. Nature 1994;371:513–515. [PubMed: 7935764]

Heidelberger R, Matthews G. Calcium influx and calcium current in single synaptic terminals of goldfish retinal bipolar neurons. J Physiol 1992;447:235–256. [PubMed: 1317429]

Heidelberger R, Sterling P, Matthews G. Roles of ATP in depletion and replenishment of the releasable pool of synaptic vesicles. J Neurophysiol 2002a;88:98–106. [PubMed: 12091535]

Heidelberger R, Thoreson WB, Witkovsky P. Synaptic transmission at retinal ribbon synapses. Prog Retin Eye Res 2005;24:682–720. [PubMed: 16027025]

Heidelberger R, Zhou ZY, Matthews G. Multiple components of membrane retrieval in synaptic terminals revealed by changes in hydrostatic pressure. J Neurophysiol 2002b;88:2509–2517. [PubMed: 12424290]

Holt M, Cooke A, Neef A, Lagnado L. High mobility of vesicles supports continuous exocytosis at a ribbon synapse. Curr Biol 2004;14:173–183. [PubMed: 14761649]

Horrigan FT, Bookman RJ. Releasable pools and the kinetics of exocytosis in adrenal chromaffin cells. Neuron 1994;13:1119–1129. [PubMed: 7946349]

Hsu SF, Jackson MB. Rapid exocytosis and endocytosis in nerve terminals of the rat posterior pituitary. J Physiol 1996;494(Pt 2):539–553. [PubMed: 8842011]

Hull C, Studholme K, Yazulla S, von GH. Diurnal changes in exocytosis and the number of synaptic ribbons at active zones of an ON-type bipolar cell terminal. J Neurophysiol 2006;96:2025–2033. [PubMed: 16738212]

Ishida AT, Stell WK, Lightfoot DO. Rod and cone inputs to bipolar cells in goldfish retina. J Comp Neurol 1980;191:315–335. [PubMed: 7410596]

Jockusch WJ, Praefcke GJ, McMahon HT, Lagnado L. Clathrin-dependent and clathrin-independent retrieval of synaptic vesicles in retinal bipolar cells. Neuron 2005;46:869–878. [PubMed: 15953416]

Joselevitch C, Kamermans M. Interaction between rod and cone inputs in mixed-input bipolar cells in goldfish retina. J Neurosci Res 2007;85:1579–1591. [PubMed: 17342779]

Kolb H, Nelson R. Rod pathways in the retina of the cat. Vision Res 1983;23:301–312. [PubMed: 6880030]

Kreft M, Krizaj D, Grilc S, Zorec R. Properties of exocytotic response in vertebrate photoreceptors. J Neurophysiol 2003;90:218–225. [PubMed: 12660355]

Kushmerick C, Renden R, von Gersdorff H. Physiological temperatures reduce the rate of vesicle pool depletion and short-term depression via an acceleration of vesicle recruitment. J Neurosci 2006;26:1366–1377. [PubMed: 16452660]

LoGiudice L, Sterling P, Matthews G. Mobility and turnover of vesicles at the synaptic ribbon. J Neurosci 2008;28:3150–3158. [PubMed: 18354018]

Mennerick S, Matthews G. Ultrafast exocytosis elicited by calcium current in synaptic terminals of retinal bipolar neurons. Neuron 1996;17:1241–1249. [PubMed: 8982170]

Messler P, Harz H, Uhl R. Instrumentation for multiwavelengths excitation imaging. J NEUROSCI METH 1996;69:137–147.

Moser T, Beutner D. Kinetics of exocytosis and endocytosis at the cochlear inner hair cell afferent synapse of the mouse. Proc Natl Acad Sci USA 2000;97:883–888. [PubMed: 10639174]

Naraghi M, Muller TH, Neher E. Two-dimensional determination of the cellular Ca^{2+} binding in bovine chromaffin cells. Biophys J 1998;75:1635–1647. [PubMed: 9746506]

Neher E. Vesicle pools and Ca^{2+} microdomains: new tools for understanding their roles in neurotransmitter release. Neuron 1998;20:389–399. [PubMed: 9539117]

Nelson R. AII amacrine cells quicken time course of rod signals in the cat retina. J Neurophysiol 1982;47:928–947. [PubMed: 6177841]

Neves G, Gomis A, Lagnado L. Calcium influx selects the fast mode of endocytosis in the synaptic terminal of retinal bipolar cells. Proc Natl Acad Sci USA 2001;98:15282–15287. [PubMed: 11734626]

Neves G, Lagnado L. The kinetics of exocytosis and endocytosis in the synaptic terminal of goldfish retinal bipolar cells. J Physiol 1999;515(Pt 1):181–202. [PubMed: 9925888]

Paillart C, Li J, Matthews G, Sterling P. Endocytosis and Vesicle Recycling at a Ribbon Synapse. J Neurosci 2003;23:4092–4099. [PubMed: 12764096]

Pan ZH, Hu HJ, Perring P, Andrade R. T-type Ca^{2+} channels mediate neurotransmitter release in retinal bipolar cells. Neuron 2001;32:89–98. [PubMed: 11604141]

Pang JJ, Gao F, Wu SM. Light-evoked current responses in rod bipolar cells, cone depolarizing bipolar cells and AII amacrine cells in dark-adapted mouse retina. J Physiol 2004;558:897–912. [PubMed: 15181169]

Protti DA, Flores-Herr N, von Gersdorff H. Light evokes Ca^{2+} spikes in the axon terminal of a retinal bipolar cell. Neuron 2000;25:215–227. [PubMed: 10707985]

Pyott SJ, Rosenmund C. The effects of temperature on vesicular supply and release in autaptic cultures of rat and mouse hippocampal neurons. J Physiol 2002;539:523–535. [PubMed: 11882684]

Rabl K, Cadetti L, Thoreson WB. Kinetics of exocytosis is faster in cones than in rods. J Neurosci 2005;25:4633–4640. [PubMed: 15872111]

Renden R, von Gersdorff H. Synaptic vesicle endocytosis at a CNS nerve terminal: faster kinetics at physiological temperatures and increased endocytotic capacity during maturation. J Neurophysiol 2007;98:3349–3359. [PubMed: 17942618]

Richards DA, Guatimosim C, Rizzoli SO, Betz WJ. Synaptic Vesicle Pools at the Frog Neuromuscular Junction. Neuron 2003;39:529–541. [PubMed: 12895425]

Rouze NC, Schwartz EA. Continuous and Transient Vesicle Cycling at a Ribbon Synapse. J Neurosci 1998;18:8614–8624. [PubMed: 9786969]

Saito T, Kujiraoka T. Physiological and morphological identification of two types of on-center bipolar cells in the carp retina. J Comp Neurol 1982;205:161–170. [PubMed: 7076890]

Sakaba T, Tachibana M, Matsui K, Minami N. Two components of transmitter release in retinal bipolar cells: exocytosis and mobilization of synaptic vesicles. Neurosci Res 1997;27:357–370. [PubMed: 9152048]

Schmitz F, Konigstorfer A, Sudhof TC. RIBEYE, a component of synaptic ribbons: a protein's journey through evolution provides insight into synaptic ribbon function. Neuron 2000;28:857–872. [PubMed: 11163272]

Singer JH, Diamond JS. Sustained Ca^{2+} entry elicits transient postsynaptic currents at a retinal ribbon synapse. J Neurosci 2003;23:10923–10933. [PubMed: 14645488]

Singer JH, Diamond JS. Vesicle depletion and synaptic depression at a mammalian ribbon synapse. J Neurophysiol 2006;95:3191–3198. [PubMed: 16452253]

Singer JH, Lassova L, Vardi N, Diamond JS. Coordinated multivesicular release at a mammalian ribbon synapse. Nat Neurosci 2004;7:826–833. [PubMed: 15235608]

Spiwoks-Becker I, Vollrath L, Seeliger MW, Jaissle G, Eshkind LG, Leube RE. Synaptic vesicle alterations in rod photoreceptors of synaptophysin-deficient mice. Neuroscience 2001;107:127–142. [PubMed: 11744253]

Stell WK, Ishida AT, Lightfoot DO. Structural basis for on-and off-center responses in retinal bipolar cells. Science 1977;198:1269–1271. [PubMed: 201028]

Sterling P, Matthews G. Structure and function of ribbon synapses. Trends Neurosci 2005;28:20–29. [PubMed: 15626493]

Sun JY, Wu LG. Fast Kinetics of Exocytosis Revealed by Simultaneous Measurements of Presynaptic Capacitance and Postsynaptic Currents at a Central Synapse. Neuron 2001;30:171–182. [PubMed: 11343653]

Thoreson WB, Rabl K, Townes-Anderson E, Heidelberger R. A highly Ca^{2+}-sensitive pool of vesicles contributes to linearity at the rod photoreceptor ribbon synapse. Neuron 2004;42:595–605. [PubMed: 15157421]

tom Dieck S, Altrock WD, Kessels MM, Qualmann B, Regus H, Brauner D, Fejtova A, Bracko O, Gundelfinger ED, Brandstatter JH. Molecular dissection of the photoreceptor ribbon synapse: physical interaction of Bassoon and RIBEYE is essential for the assembly of the ribbon complex. J Cell Biol 2005;168:825–836. [PubMed: 15728193]

Trexler EB, Li W, Massey SC. Simultaneous Contribution of Two Rod Pathways to AII Amacrine and Cone Bipolar Cell Light Responses. J Neurophysiol 2005;93:1476–1485. [PubMed: 15525810]

Tsukamoto Y, Morigiwa K, Ueda M, Sterling P. Microcircuits for night vision in mouse retina. J Neurosci 2001;21:8616–8623. [PubMed: 11606649]

Veruki ML, Hartveit E. Electrical Synapses Mediate Signal Transmission in the Rod Pathway of the Mammalian Retina. J Neurosci 2002;22:10558–10566. [PubMed: 12486148]

Veruki ML, Morkve SH, Hartveit E. Functional properties of spontaneous EPSCs and non-NMDA receptors in rod amacrine (AII) cells in the rat retina. J Physiol 2003;549:759–774. [PubMed: 12702738]

von Gersdorff H. Synaptic ribbons: versatile signal transducers. Neuron 2001;29:7–10. [PubMed: 11182076]

von Gersdorff H, Matthews G. Dynamics of synaptic vesicle fusion and membrane retrieval in synaptic terminals. Nature 1994a;367:735–739. [PubMed: 7906397]

von Gersdorff H, Matthews G. Inhibition of endocytosis by elevated internal calcium in a synaptic terminal. Nature 1994b;370:652–655. [PubMed: 8065451]

von Gersdorff H, Matthews G. Depletion and replenishment of vesicle pools at a ribbon-type synaptic terminal. J Neurosci 1997;17:1919–1927. [PubMed: 9045721]

von Gersdorff H, Sakaba T, Berglund K, Tachibana M. Submillisecond kinetics of glutamate release from a sensory synapse. Neuron 1998;21:1177–1188. [PubMed: 9856472]

von Gersdorff H, Vardi E, Matthews G, Sterling P. Evidence that vesicles on the synaptic ribbon of retinal bipolar neurons can be rapidly released. Neuron 1996;16:1221–1227. [PubMed: 8663998]

Wadel K, Neher E, Sakaba T. The Coupling between Synaptic Vesicles and Ca^{2+} Channels Determines Fast Neurotransmitter Release. Neuron 2007;53:563–575. [PubMed: 17296557]

Wang MM, Janz R, Belizaire R, Frishman LJ, Sherry DM. Differential distribution and developmental expression of synaptic vesicle protein 2 isoforms in the mouse retina. J Comp Neurol 2003;460:106–122. [PubMed: 12687700]

Witkovsky P, Dowling JE. Synaptic relationships in the plexiform layers of carp retina. Z Zellforsch Mikrosk Anat 1969;100:60–82. [PubMed: 5354186]

Wu LG. Kinetic regulation of vesicle endocytosis at synapses. Trends Neurosci 2004;27:548–554. [PubMed: 15331237]

Wu LG, Betz WJ. Nerve activity but not intracellular calcium determines the time course of endocytosis at the frog neuromuscular junction. Neuron 1996;17:769–779. [PubMed: 8893033]

Zenisek D, Horst NK, Merrifield C, Sterling P, Matthews G. Visualizing synaptic ribbons in the living cell. J Neurosci 2004;24:9752–9759. [PubMed: 15525760]

Zenisek D, Steyer JA, Almers W. Transport, capture and exocytosis of single synaptic vesicles at active zones. Nature 2000;406:849–854. [PubMed: 10972279]

Zhou ZY, Wan QF, Thakur P, Heidelberger R. Capacitance measurements in the mouse rod bipolar cell identify a pool of releasable synaptic vesicles. J Neurophysiol 2006;96:2539–2548. [PubMed: 16914610]
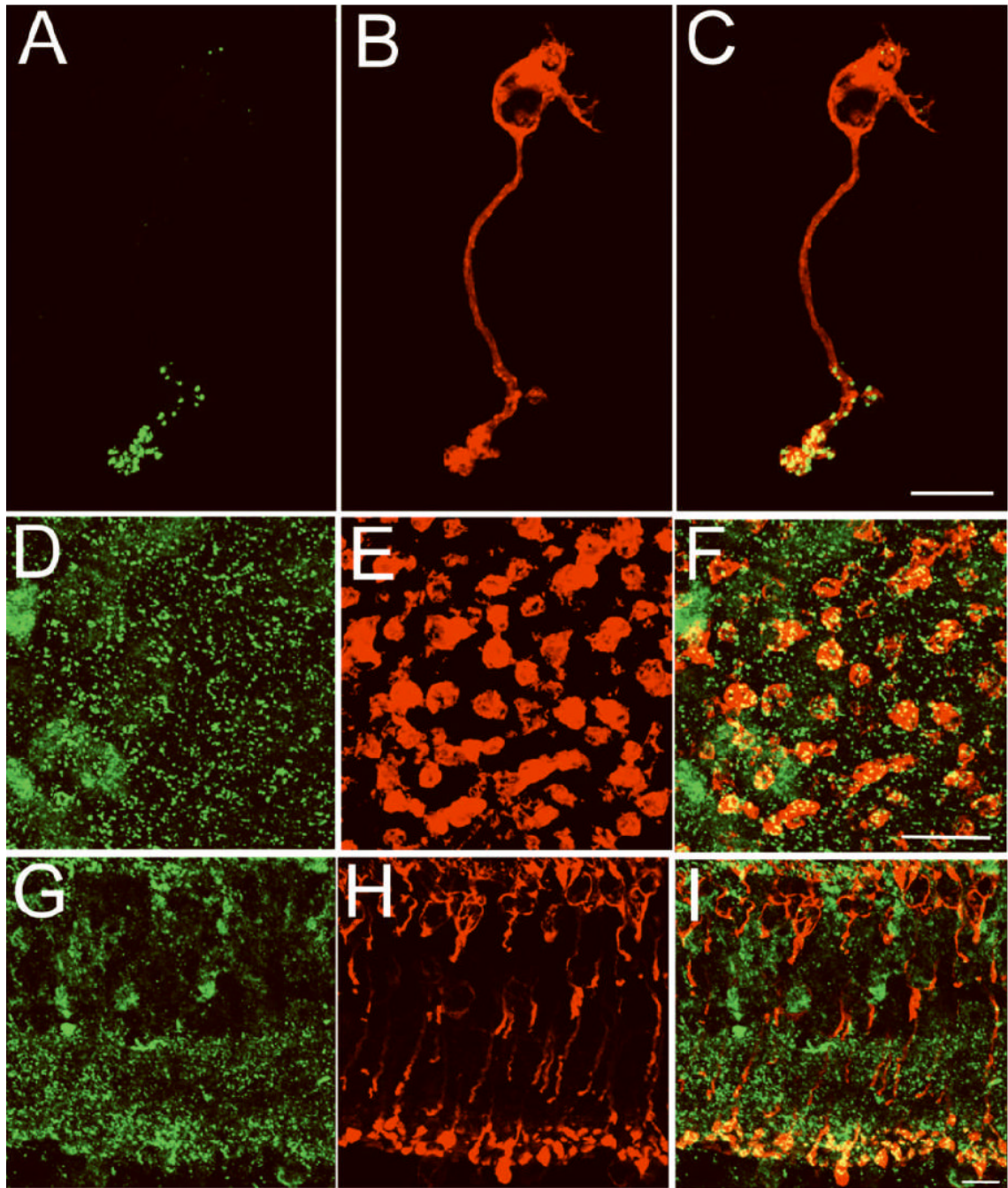
Figure 1. An isolated rod bipolar cell contains ≈ 34 synaptic ribbons
Confocal fluorescence images of a freshly isolated mouse rod bipolar cell (A-C), a whole mount
retinal section (D-F) in the lower sublamina of the inner plexiform layer (IPL) and a retinal
vertical section (G-I) were double-labeled for CtBP2/ribeye (green, A, D,G) and PKC-α (red,
B, E, H). CtBP2/ribeye marks the synaptic ribbon, while PKC-α labels rod bipolar cells. CtBP2/
ribeye immunofluorescence (green) is prominent in the synaptic terminals of isolated rod
bipolar cells and in the IPL, the retinal layer in which the terminals of all bipolar cells reside.
The number of synaptic ribbons in a rod bipolar cell was determined from the number of CtBP2/
ribeye puncta that resided within the terminal cluster of an individual isolated PKC-α positive
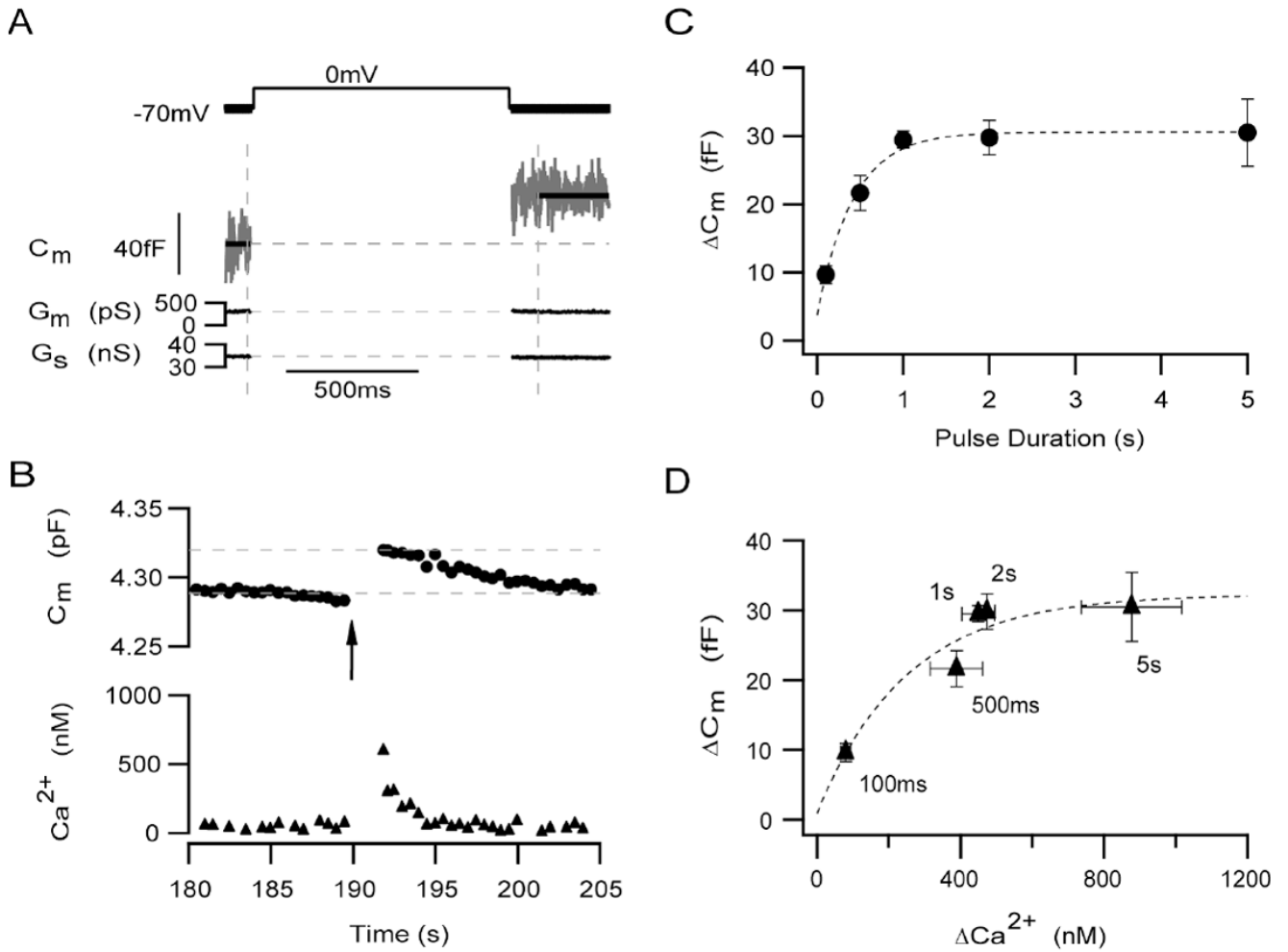bipolar cell (34 ± 4; n=10). Scale bars represent 10 μm.

Figure 2. A 1 s depolarization is sufficient to deplete the entire releasable pool
(A) A typical example of high-resolution capacitance recording shows the increase in C_m (middle traces) stimulated by a 1 s depolarization from -70 to 0 mV (upper trace). The first dashed vertical line indicates the onset of the depolarization (middle and lower traces). Beginning about 25 ms after the end of the depolarization (second dashed vertical line), changes in G_m and G_s (lower traces), were not correlated with changes in C_m. (B) The corresponding time-resolved capacitance (upper traces, circles) and calcium (bottom traces, triangles) records for the same neuron shown in A. Arrow marks the onset of the depolarization. Calcium record obtained selectively from synaptic terminal (Zhou *et al.*, 2006). (C) The amplitude of release increased with pulse duration until a plateau was reached at a pulse duration of $\approx$ 1 s. The time course of vesicles depletion from this pool was best described by a single exponential function (dashed curve) given by: $Y = Y_0 + Ae^{(-x/\tau_1)}$, where $Y_0 = 30.6 \pm 0.8$, $A = -26.8 \pm 2.0$, and $\tau_1 = 0.417 \pm 0.071$). For (C) and (D), for a 100 ms depolarization: $\Delta C_m = 9.6 \pm 1.3$ fF, $\Delta[Ca^{2+}]_i = 79 \pm 14$ nM; n = 14. For 500 ms: $\Delta C_m = 21.6 \pm 2.8$ fF, $\Delta[Ca^{2+}]_i = 434 \pm 71$ nM; n = 14. For 1 s: $\Delta C_m = 29.5 \pm 1.2$ fF, $\Delta[Ca^{2+}]_i = 449 \pm 46$ nM; n = 79. For 2 s: $\Delta C_m = 29.8 \pm 2.5$ fF, $\Delta[Ca^{2+}]_i = 473 \pm 22$ nM; n = 10. For 5 s: $\Delta C_m = 30.5 \pm 4.9$ fF, $\Delta[Ca^{2+}]_i = 877 \pm 140$ nM; n = 8. Error bars represent SEM. (D) With increasing pulse duration, the magnitude of the rise in intraterminal Ca^{2+} also increases. For each pulse duration, the average change in C_m is plotted against the average rise in intraterminal Ca^{2+}. The data suggest that either a 1 s voltage from -70 to 0 mV or elevating intraterminal Ca^{2+} to about 450 nM is sufficient to deplete the

entire releasable pool. The grey curve is fitted to the data using the equation $Y = Y_0 + Ae^{(-(x-x0)/\tau^1)}$, where $Y_0 = 32.3 \pm 5.6$, $X_0 = 79.4$, $A = -22.8 \pm 6.5$, and $\tau_1 = 250 \pm 169$.
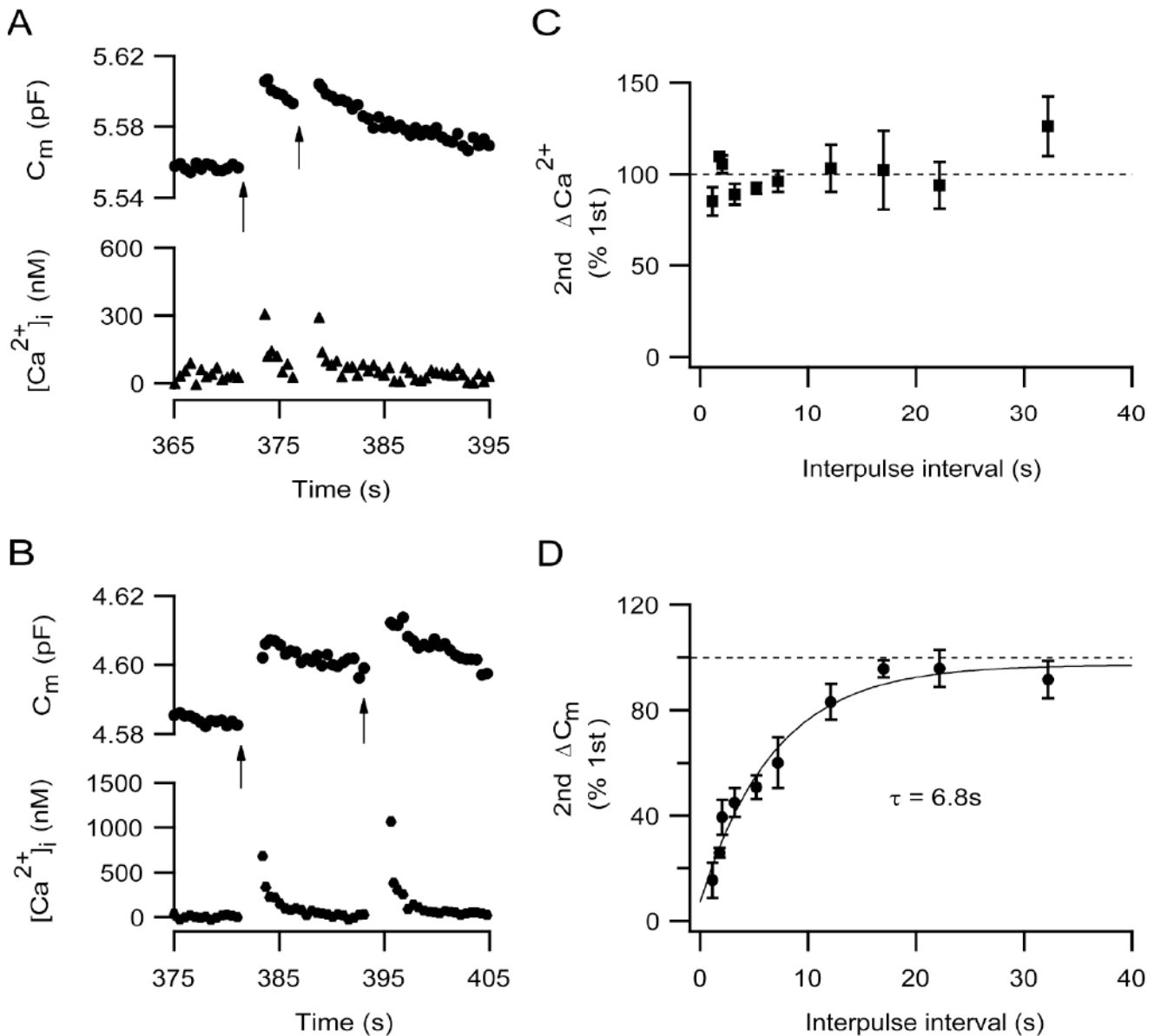
Figure 3. Complete recovery from paired-pulse depression of the releasable pool requires ≈ 21 seconds

(A). Two 1 s depolarizations (-70 to 0 mV), separated by 5.2 s were given to an isolated mouse rod bipolar cell (arrows). The upper trace (circles) shows the capacitance record and the lower trace (triangles) show the spatially-averaged intraterminal Ca^{2+}. (B). Two 1 s depolarizations (-70 to 0 mV), separated by 12.1 s were given to an isolated mouse rod bipolar cell (arrows). The upper trace (circles) shows the capacitance record and the lower trace (triangles) show the spatially-averaged intraterminal Ca^{2+}. (C) The second increase in intraterminal calcium as a percentage of the first is plotted against the interpulse interval. The percentage of the second calcium transient relative to the first hovered about 100%, indicating that intraterminal calcium signaling was not depressed at the time of the second pulse. (D) The second capacitance response as a percentage of the first is plotted against the interpulse interval. The time course of refilling was described by a single exponential function (solid curve) given by the equation: $(Y = Y_0 + A_1 e^{(-x/\tau^1)}$, where $Y_0 = 97.3 \pm 5.0$, $A_1 = -90.2 \pm 6.3$, $\tau_1 = 6.8 \pm 1.5$). (Interpulse

interval, number of cells: 1.12 s, n = 5; 1.8 s, n = 3; 2.02 s, n = 7; 3.2 s, n = 8; 5.2 s, n = 6; 7.2 s, n = 6; 12.1 s, n = 7; 17 s, n = 5; 22 s, n = 7; 32 s, n = 6). Error bars represent SEM.
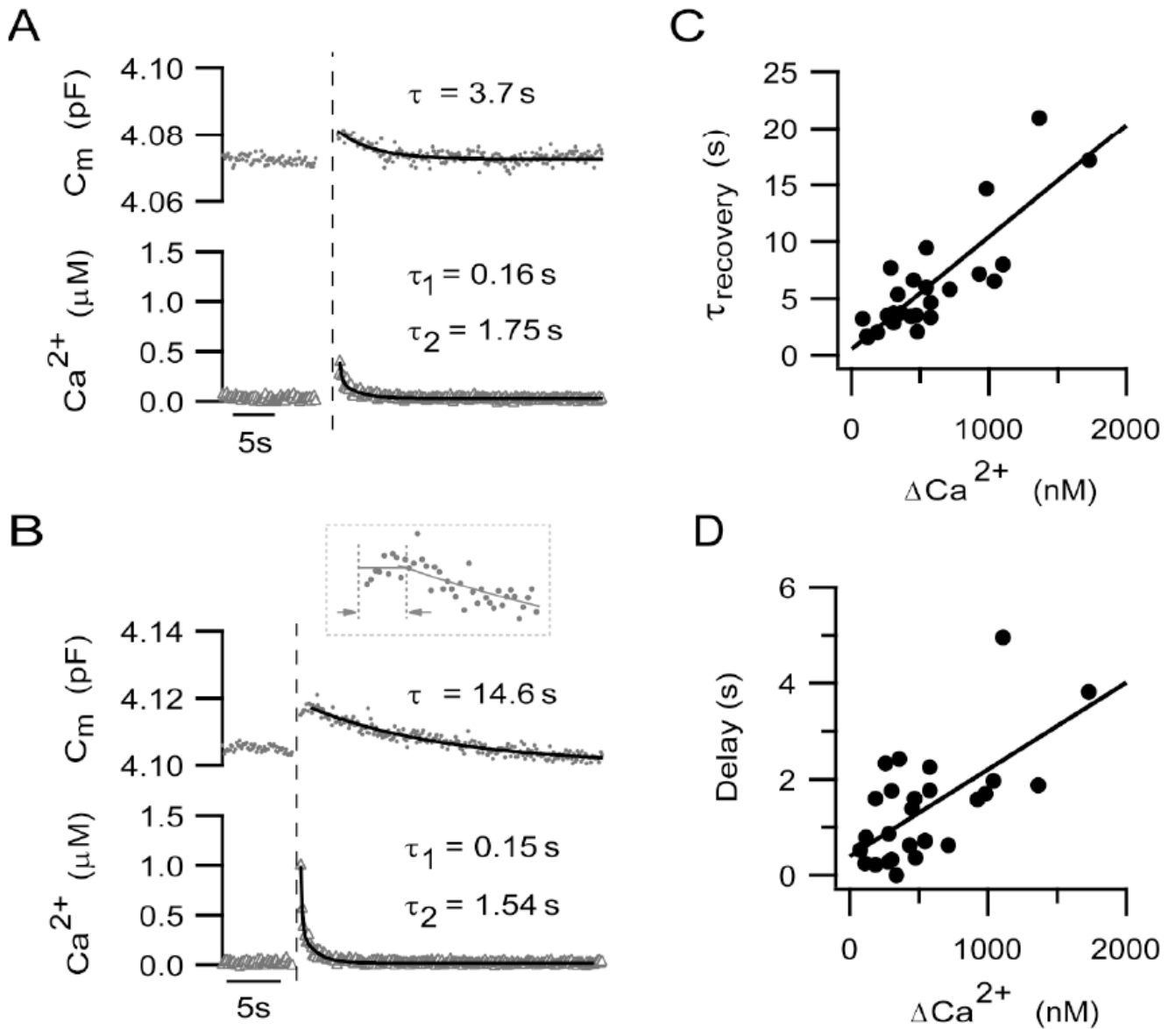
Figure 4. The time course and onset of membrane recovery is calcium-dependent
(A-B) Examples of secretory responses (upper traces, capacitance response, circles; lower traces, calcium response, triangles) evoked by a 500 ms pulse from -70 to 0 mV. The vertical dashed lines mark the end of the depolarization. The time constant of membrane recovery was derived from the single exponential fit to the capacitance decay (superimposed curves with indicated time constants). The inset in B shows the first ≈ 6 s of the capacitance record from the end of the depolarization (first vertical dashed line) on an expanded time scale. The delay in onset of membrane recovery was measured as the time between the first vertical line and the second. The second dashed line marks the time point at which the exponential fit to the falling phase intercepts the average magnitude of the capacitance response, given by the horizontal line. Recovery of calcium transients to baseline were described by the following double exponential functions (superimposed curves), $Y = Y_0 + A_1 e^{(-x/\tau^1)} + A_2 e^{(-x/\tau^2)}$, where in Fig. 4A, $Y_0 = 0.031 \pm 0.003$, $A_1 = 0.47 \pm 0.15$, $\tau_1 = 0.16 \pm 0.06$, $A_2 = 0.19 \pm 0.03$, $\tau_2 = 1.75 \pm 0.29$. In Fig. 4B, $Y_0 = 0.018 \pm 0.001$, $A_1 = 0.66 \pm 0.03$, $\tau_1 = 0.15 \pm 0.01$, $A_2 = 0.33 \pm 0.02$,

$\tau_2 = 1.54 \pm 0.11$. Note that the neuron with the larger Ca^{2+} transient exhibited a slower time course of C_m recovery. (C) The time constant of membrane recovery increased as a function of the magnitude of the Ca^{2+} transient, $\Delta[Ca^{2+}]_i$. The relationship is decreased by a line given by: $Y = a + bX$, where $a = 0.51 \pm 0.86$ and $b = 0.0099 \pm 0.0013$. The correlation of determination, r^2, $= 0.71$. The slope given by b is significantly different from zero (p<0.0001). (D) The delay in the onset of membrane recovery is plotted against $\Delta[Ca^{2+}]_i$. The delay became longer with increasing $\Delta[Ca^{2+}]_i$. This relationship can be described by a line given by the equation: $Y = a + bX$, where $a = 0.39 \pm 0.29$, $b = 0.0018 \pm 0.00043$. $R^2 = 0.41$, and the slope b is significantly different from zero (p= 0.0003).